An Along-the-Channel Model for Proton Exchange Membrane Fuel Cells

Article *in* Journal of The Electrochemical Society · April 1998

DOI: 10.1149/1.1838431

2 authors:

Jung S. Yi
Pynus Cable
34 PUBLICATIONS **2,992** CITATIONS

SEE PROFILE

Trung Van Nguyen
University of Kansas
124 PUBLICATIONS **6,784** CITATIONS

SEE PROFILE

An Along-the-Channel Model for Proton Exchange Membrane Fuel Cells

Jung S. Yi* and Trung V. Nguyen**

Department of Chemical and Petroleum Engineering, University of Kansas, Lawrence, Kansas 66045, USA

ABSTRACT

An along-the-channel model is developed for evaluating the effects of various design and operating parameters on the performance of a proton exchange membrane (PEM) fuel cell. The model, which is based on a previous one, has been extended to include the convective water transport across the membrane by a pressure gradient, temperature distribution in the solid phase along the flow channel, and heat removal by natural convection and coflow and counterflow heat exchangers. Results from the model show that the performance of a PEM fuel cell could be improved by anode humidification and positive differential pressure between the cathode and anode to increase the back transport rate of water across the membrane. Results also show that effective heat removal is necessary for preventing excessive temperature which could lead to local membrane dehydration. For heat removal and distribution, the counterflow heat exchanger is most effective.

Introduction

With increasing environmental concerns over vehicle generated pollution and the limited range associated with battery powered electric vehicles, the proton exchange membrane (PEM) fuel cell system is gaining more attention as an alternative power generation source for electric vehicles. Attractive characteristics of the PEM fuel cell system include the simplicity of its design and operation, self-starting at low temperatures, low cost construction materials, CO_2 tolerance, and driving range and refueling time comparable to conventionally powered vehicles.

Recent interest in this system has resulted in extensive studies on increasing the catalytic activity and utilization of platinum-supported gas diffusion electrodes. Efforts in sputtering the catalyst onto the surface of the electrode that is later hot-pressed onto the membrane and mixing the catalyst substrate with membrane material have resulted in significant improvement in fuel cell performance and reduction in the catalyst loading. The catalyst loading has decreased from as high as 5 mg Pt/cm^2 to less than 0.05 mg Pt/cm^2.[1,2] These studies have also resulted in a better understanding of the important role of the membrane water and ionic transport properties and heat and water management in the system performance and stability in prolonged operations.

During PEM fuel cell operations, water molecules are carried from the anode side to the cathode side of the membrane by electro-osmosis, and if this transport rate of water is higher than that by back diffusion of water, the membrane will become dehydrated and too resistive to conduct high current. On the other hand, at the cathode side of the membrane where water molecules are not only transported from the anode side but also generated by the cathodic reaction, electrode flooding occurs when the water removal rate fails to keep up with its transport rate out of the electrode. Consequently, a sufficient amount of water must be added to the anode stream to make up for the amount of water lost due to the net transport of water from the anode to the cathode, and water must be removed from the cathode side of the membrane to maintain an active catalyst surface for reaction. To maintain high membrane conductivity and prevent flooding at the cathode, proper water management is required. Moreover, the effect of reacting gas dilution by high water vapor pressure must also be taken into consideration.[3]

Next, even though a PEM fuel cell is a very efficient system, there is still 40-50% of the energy produced dissipated as heat.[4] This thermal generation is due to the irreversibility of the cathodic reaction, ohmic resistance, and mass-transport overpotentials. The thermal distribution has a strong impact on the fuel cell performance by affecting the transport of water and gaseous species as well as the electrochemical reactions in the electrodes. Furthermore, it may give rise to excessive cell temperature and, consequently, membrane dehydration or shrinkage and rupture of the membrane. Therefore, proper water and thermal management is necessary for achieving high performance and efficiency.[5]

Efficient water and thermal management can be accomplished by a number of approaches that include operating conditions, fuel cell hardware, and membrane electrode assembly designs. Among the different humidification designs to prevent dehydration at the anode side of the membrane discussed by Nguyen and White,[6] the liquid water injection scheme could be used as a water and thermal management strategy. In their studies, the results show that injecting liquid water into the anode flow channels could improve the cell performance by providing not only humidification to keep the anode side of the membrane hydrated, but also simultaneous heat removal. Also, it was shown that when air was used, because of the higher gaseous flow rates, the cathode stream must also be humidified to prevent dehydration of the cathode layers near the entrance, the region of highest activity. Vanderborgh et al.[4] discussed designs that include recirculation gas fans, humidifiers, and heat exchangers to provide humidification for the anode and water and heat removal for the cathode. Wicking materials were also proposed by Watanabe et al.[7] as a way to remove water from the cathode.

In search of better fuel-cell designs and operation strategies, numerous models of PEM fuel cells at different levels of complexity have been developed.[8-11] However, by treating the flow channels in the fuel cells to be perfectly well mixed, these models cannot account for the effects of the depletion of the reactants, production of water, and temperature distribution along the length of the fuel cell. Proper water and thermal management for PEM fuel cells needs to account for these changes along the fuel cells. Fuller and Newman[12] and Nguyen and White[6] have developed two-dimensional heat and water transport models that account for variations in the gas-phase compositions and temperature and membrane hydration condition along the channels. Results from Fuller and Newman's model[12] showed that adequate heat removal is essential for preventing membrane dehydration and maintain high performance. Nguyen and White[6] used the model to investigate the effectiveness of various humidification systems in maintaining high membrane hydration and performance for PEM fuel cells. However, in their model,[6] the temperature of the solid phase (flow channel plates, electrodes, and membrane) was assumed to be uniform and constant. In practice, there is a significant temperature gradient in the solid layers along the flow channels of the fuel cell,[13] and this difference affects the temperature distribution of the fluid in the flow channels and the hydration state of

* Electrochemical Society Student Member.
** Electrochemical Society Active Member.

the membrane along the flow path. These effects are very important components of stack and system design and can have a major impact on the overall system power, cost, efficiency, and control. To address these problems better, a new model is developed based on Nguyen and White's model to describe mass and thermal conditions in both the solid and gas phases along the flow path of both the anode and cathode faces of a PEM fuel cell.

Model Development

A two-dimensional, steady-state, mass and energy model for a PEM fuel cell is developed. The model regions, consisting of the anode flow channels, cathode flow channels, and solid phases representing the membrane/electrode assembly and flow distributors are shown in Fig. 1. The model accounts for the presence of multiple channels on each side of the flow fields, mass transport of water and gaseous species across the cell (y direction) and along the flow channels (x direction), and heat transport in the gaseous and solid phases of the cell along the flow path (x direction).

Assumptions.—In the flow channels, a plug-flow condition is assumed, and pressure drop along the channels is neglected. For the gaseous species the ideal gas law is used. The liquid water is assumed to exist at the surface of the channels, and its volume is assumed to be negligible. Water transport in and out of the electrodes is assumed to be in the form of vapor only. This assumption is probably the weakest assumption of the model, especially for the cathode. The water generation rate at high current density is very likely to exceed its removal rate from the inner layers by gas diffusion and, consequently, results in condensation and flooding of the electrode. This complexity, which is neglected here, will be considered in our future work when we take into account two-phase flow in porous media. It is assumed that the electrode layers are ultrathin, so that gas transport resistance through the electrode porous layer can be neglected. With these assumptions, the properties at the faces of the membrane are determined by the conditions in the channels. Next, since the thickness of the cell (SH) is relatively small compared to the length of the channel (L), it is assumed here that there is no temperature drop in the solid phase across the cell (y direction). With the anode side of the membrane more likely to be drier than the cathode side due to the positive net water transport from the anode to the cathode at high current densities, the electro-osmotic coefficient and the diffusion coefficient of water in the membrane are assumed to be determined by the activity of the water in the anode flow channel. Finally, because of the high electrical conductivity of the current collectors, no potential drop along the channels is assumed. Also, anode and cathode gas flows are assumed to be coflow or parallel to each other.

Cell performance.—The performance of a fuel cell is represented by the current density and potential relation. Ideally, a single PEM fuel cell could produce 1.1 V at ambient conditions. In practice, however, its potential outputs are less than ideal and decrease with increasing current density. The potential difference between the cell output potential and its open-circuit potential is attributed to the electrode overpotentials (η) and membrane resistance and current density [$t_m I(x)/\sigma_m$], The depletion of the reactant gases and production of water at the cathode result in changing local current densities [$I(x)$], membrane conductivity, and electrode overpotential along the channels. The same relation for potential and current density and expressions for the electrode overpotential and membrane conductivity used by Nguyen and White[6] are employed. Since the membrane tends to be drier at the anode side, the conductivity of the membrane and the water concentration in the membrane [$c_w(x)$] are estimated using the conditions in the anode channels.

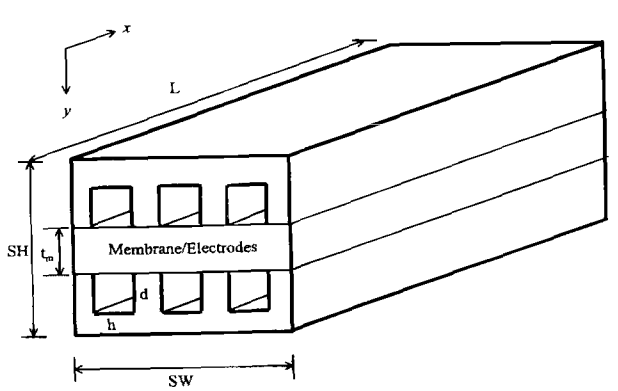

Fig. 1. Schematic diagram of modeling region.

Flow channels.—The change in the molar flow rate of a single-phase species i along the channel length is due to its normal flux in the y direction into or out of the membrane. The change in the molar flow rates of water vapor along the flow channels depends on both the changes in the liquid water and the flux of water vapor in and out of the membrane. Expressions for the molar flow rates of various species existing in the channels are the same as those in Ref. 6. The energy balance equation for the anode and cathode gaseous streams is

$$\sum_i \{M_i(x)C_{p,i}(x)\}\frac{dT_k(x)}{dx} = Ua\{T_s(x) - T_k(x)\} \qquad [1]$$

where the subscript k represents either the anode or cathode, and i is for gaseous species existing in the channels. The parameter U is the overall heat-transfer coefficient, and the parameter a is the heat-transfer area per unit length of the flow channel. The term on the right side of Eq. 1 accounts for the energy transported from the fluid in the channel to the solid layer of the cell. Expressions for the heat capacity of each component, $C_{p,i}$, are given in Ref. 6.

Membrane.—As was explained earlier, the net water flux [$N_{w,y,m}(x)$] through the membrane from the anode side to the cathode side is proportional to the local current density, $I(x)$, generated at that position. Water transport through the membrane can be described by three transport mechanisms: (*i*) electro-osmotic drag, which is caused by proton transport from the anode side to the cathode side of the membrane, (*ii*) back-diffusion by the concentration gradient of water created by the electro-osmotic flow from the anode side to the cathode side and the cathodic reaction, and (*iii*) convection by pressure gradient between the anode side and the cathode side of the channels. Therefore, the water flux through the membrane (y direction) can be written as follows

$$N_{w,y,m}(x) = n_d(x)\frac{I(x)}{F} - D_w(x)\frac{dc_w(x)}{dy} - c_w(x)\frac{k_p}{\mu}\frac{dP_w(x)}{dy} \qquad [2]$$

where n_d, D_w, k_p, and μ are the electro-osmotic drag coefficient, diffusion coefficient of water, permeability of water in the membrane, and water viscosity, respectively. Next, Eq. 2 can be rearranged to yield the expression for the net water molecules per proton flux ratio, α, as follows

$$\alpha = n_d - D_w\frac{F}{I(x)}\frac{dc_w}{dy} - c_w\frac{k_p}{\mu}\frac{F}{I(x)}\frac{dP_w}{dy} \qquad [3]$$

Since the membrane is very thin (≈0.01 cm), the single-step linear difference assumption between the anode side and cathode side is used for the concentration and pressure gradients of water across the membrane. Also, the water concentration in the membrane can be estimated by taking the algebraic mean of the concentration of water in the anode and the cathode sides of the membrane. Therefore, Eq. 3 can be changed to the following form

$$\alpha(x) = n_d(x) - D_w(x)\frac{F}{I(x)}\frac{\{c_{w,c}(x) - c_{w,a}(x)\}}{t_m}$$

$$- \frac{\{c_{w,c}(x) + c_{w,a}(x)\}}{2}\frac{k_p}{\mu}\frac{F}{I(x)}\frac{\{P_{w,c}(x) - P_{w,a}(x)\}}{t_m} \quad [4]$$

where $c_{w,a}(x)$ and $c_{w,c}(x)$ are the concentration of water in the anode and the cathode channels, and $P_{w,a}(x)$ and $P_{w,c}(x)$ are the water vapor pressure in the anode and the cathode channels, respectively. Parameter t_m is the thickness of the membrane.

The electro-osmotic coefficient and the diffusion coefficient of water depend on the water content in the membrane, and they change along the channels as the water vapor condition in the channels varies. The correlations for the dependence of the diffusion coefficient of water and the electro-osmotic coefficient on water from Ref. 6 are used. However, since the permeability of water in the membrane is not sensitive to the water content and remains reasonably constant through the temperatures below the glass transition temperature of the membrane,[14] it is assumed constant for all water contents and temperatures in this work.

In a PEM fuel cell, the water content in the membrane depends on the activity of water in the gas phase next to the membrane, and the activities of water in the gas phases of each side of the membrane are different because the anode tends to be dehydrated and cathode overhydrated during operation. With the approach used here to describe the flux of water across the membrane, it is difficult to determine what value to use for the water content in the membrane for different environmental conditions on each side of the membrane. Three different schemes have been tested using: (*i*) the water activity in the anode channels (this is the approach used by Ref. 6), (*ii*) the water activity in the cathode channels, or (*iii*) averaged values of anode activity and cathode activity in the channels. When the cathode water activity and anode-cathode averaged activity are used, the current and potential relations show much higher performance than those shown in published results from others and our own experimental results. Therefore, the anode water activity is used to estimate the water content of the membrane to evaluate the electro-osmotic coefficient and diffusion coefficient for all calculations in the work. This approach is deemed reasonable because the transport of water in the membrane is most likely to be limited by the anode side unless the cathode somehow becomes dehydrated, which is only possible with very high dry air or oxygen flow rates, a highly unlikely mode of operation.

Zawodzinski et al.[15] measured the relation between the water vapor activity and the membrane water content at 30°C in a condition in which the membrane is surrounded by water vapor. However, during a fuel cell operation, the existing phase of water at the faces of the membrane is not really known. Chances that water contacts the membrane as a liquid are very likely at the cathode. Springer et al.[11] found that when the membrane is immersed in liquid water, the water content can go as high as 16.8 water molecules per ionic site at 80°C. This observation along with the results from Zawodzinski et al.[15] suggests the cubic correlation used in previous modeling works.[6,11] Note that in this correlation water contents are estimated even when the water activity goes above 1. However, since the activities of water vapor in the cell are either at one or less, the correlation for activities above one does not contribute to the results. Also, since the cubic correlation is very complicated, using it frequently results in instability in the calculation and gives discontinuous results for some conditions. To prevent the instability and discontinuous problems, the simple linear relation which is shown below is proposed and used for all studies in this work

$$\lambda(x) = 14\ a_k(x) \quad [5]$$

Once the water content of the membrane is estimated, the water drag coefficient and the water diffusion coefficient in the membrane can be calculated by the expressions provided in Ref. 6.

Solid phase (flow plates and membrane).—When liquid water exists in the flow channel, it tends to be on the surface of the flow plate. Since heat transfer between the liquid water droplets and the flow plate is always faster than that between the liquid water droplets and the gas phase, it is assumed that the liquid and the solid phases exist at the same temperature. Therefore, when water condenses or vaporizes in the channels, it is assumed that the phase change takes place on the surface of the flow plate with energy transferred to or from the solid phase. The energy balance equation for the solid phase of the cell is

$$A_s k\frac{d^2T_s(x)}{dx^2} - n_c\{M^l_{w,a}(x) + M^l_{w,c}(x)\}C^l_{p,w}\frac{dT_s(x)}{dx}$$

$$= -n_c a U\{T_a(x) + T_c(x) - 2T_s(x)\} - A_b U_b\{T_{hef}(x) - T_s(x)\}$$

$$- n_c\{H^v_{w,a} - H^l_{w,a}\}(x)\frac{dM^l_{w,a}(x)}{dx} - n_c\{H^v_{w,c} - H^l_{w,c}\{(x)\frac{dM^l_{w,c}(x)}{dx}$$

$$+ n_c h\left\{\left[\frac{\Delta S_{H2}}{2F} + \frac{\Delta S_{O2}}{4F}\right][T_s(x) + 273] - \eta(x)\right\}I(x) \quad [6]$$

where n_c is the number of the flow channels on each side of the membrane, A_s represents the cross-sectional area of the solid layer along the flow direction, and A_b is the surface area of the solid flow distributors open for energy exchange to the surrounding. The first term on the left side of the equation represents energy flow by conduction in the solid layer of the cell along the gas flow path (x direction). The second term is for the energy flow by the liquid water along the flow channels. The temperature distribution normal to gas flow (y axis) is assumed to be uniform. The first term on the right side of the equation is for convective heat transfer between the fluid in the channels and the solid phase of cell, and the second term is for convective energy exchange between the solid layer of cell and the heat exchanger fluid temperature. If convective bulk condition is applied, $T_{hef}(x)$ is substituted for the constant bulk temperature, T_b. The third and the fourth terms account for the energy taken or released from the phase changes of water in the anode or cathode flow channels, respectively. Values for the heat of evaporation or condensation, $(H^v_{w,k} - H^l_{w,k})(x)$, as a function of temperature are from Ref. 6. The last term represents heat generation by the irreversibility and overpotential of the reactions. Since temperature distributions in the y direction are ignored, energy generated by ohmic resistance in the y-direction is neglected.

Heat exchanger designs.—To examine different heat removal and distribution designs for the fuel cell, different bulk conditions are considered. In one, constant bulk temperature (T_b) for free convection from the exterior surface of the cell is assumed, and in the other, coflow or counterflow heat exchanger designs are evaluated. In both cases, the external surface area (A_b) of the flow fields and the overall heat-transfer coefficient to bulk (U_b) must be defined for Eq. 6. When the heat exchanger designs are applied, the following equations are used as the energy balances for the heat exchanger fluid

$$MC_p\frac{dT_{hef}(x)}{dx} = U_b A_b\{T_s(x) - T_{hef}(x)\}$$

for coflow heat exchanger [7]

$$MC_p\frac{dT_{hef}(x)}{dx} = -U_b A_b\{T_s(x) - T_{hef}(x)\}$$

for counterflow heat exchanger [8]

where $T_{hef}(x)$ denotes the heat exchanger fluid temperature at position x and U_b is the overall heat-transfer coefficient between the exterior surface of the cell and the heat exchanger fluid. The parameters C_p and M represent the heat capacity and molar velocity of the heat exchanger fluid, respectively.

Boundary conditions.—The set of equations used in the model is given in Table I. There are twelve governing equations for twelve unknowns, M_{H_2}, M_{O_2}, M_{N_2}, $M^v_{w,a}$, $M^l_{w,a}$, $M^v_{w,c}$, $M^l_{w,c}$, T_a, T_c, T_s, T_{hef}, and I. The inlet conditions, at $x = 0$, for the gas species (M_{H_2}, M_{O_2}, M_{N_2}, $M^v_{w,a}$, and $M^v_{w,c}$) and liquid water ($M^l_{w,a}$, and $M^l_{w,c}$) are specified, as well as the inlet stream temperatures for the anode and cathode (T_a and T_c). When a heat exchanger is used, the inlet temperature for the heat exchanger fluid (T_{hef}) is also fixed for both the coflow and counterflow cases. Since the equation for the temperature of the solid phase is a second-order differential equation, two boundary conditions are required

$$\text{At } x = 0 \quad \frac{dT_s(x)}{dx} = -\frac{U_b}{k}\{T_b - T_s(x)\} - \frac{C^l_{p,w}M^l_{w,a}(x)}{kA_s}\{T_a(x) - T_s(x)\} - \frac{C^l_{p,w}M^l_{w,c}(x)}{kA_s}\{T_c(x) - T_s(x)\} \quad [9]$$

Table I. Governing equations for an along-the-channel model.

Hydrogen

$$\frac{dM_{H_2}(x)}{dx} = -\frac{h}{2F}I(x) \quad [T\text{-}1]$$

Anode liquid water

$$\frac{dM^l_{w,a}(x)}{dx} = \left\{\frac{k_c hd}{R[T_a(x) + 273]}\right\}\left\{\frac{M^v_{w,a}(x)}{M^v_{w,a}(x) + M_{H_2}(x)}p_a - p^{sat}_{w,a}(x)\right\} \quad [T\text{-}2]$$

Anode vapor water

$$\frac{dM^v_{w,a}(x)}{dx} = -\frac{dM^l_{w,a}(x)}{dx} - \frac{h\alpha(x)}{F}I(x) \quad [T\text{-}3]$$

Anode stream temperature

$$\{M_{H_2}(x)C_{p,H_2}(x) + M^v_{w,a}(x)C^v_{p,w,a}(x)\}\frac{dT_a(x)}{dx} = Ua\{T_s(x) - T_a(x)\} \quad [T\text{-}4]$$

Oxygen

$$\frac{dM_{O_2}(x)}{dx} = -\frac{h}{4F}I(x) \quad [T\text{-}5]$$

Nitrogen

$$M_{N_2,c} = M^0_{N_2,c} \quad [T\text{-}6]$$

Cathode liquid water

$$\frac{dM^l_{w,c}(x)}{dx} = \left\{\frac{k_c hd}{R[T_k(x) + 273]}\right\}\left\{\frac{M^v_{w,c}(x)}{M^v_{w,c}(x) + M_{O_2}(x) + M_{N_2,c}}p_c - p^{sat}_{w,c}(x)\right\} \quad [T\text{-}7]$$

Cathode vapor water

$$\frac{dM^v_{w,c}(x)}{dx} = -\frac{dM^l_{w,c}(x)}{dx} + \frac{h\{1 + 2\alpha(x)\}}{2F}I(x) \quad [T\text{-}8]$$

Cathode stream temperature

$$\{M_{O_2}(x)C_{p,O_2}(x) + M_{N_2,c}C_{p,N_2}(x) + M^v_{w,c}(x)C^v_{p,w,c}(x)\}\frac{dT_c(x)}{dx} = Ua\{T_s(x) - T_c(x)\} \quad [T\text{-}9]$$

Solid layer temperature

$$A_s k\frac{d^2T_s(x)}{dx^2} - n_c\{M^l_{w,a}(x) + M^l_{w,c}(x)\}C^l_{p,w}\frac{dT_s(x)}{dx} = -n_c aU\{T_a(x) + T_c(x) - 2T_s(x)\} - A_b U_b\{T_{hef}(x) - T_s(x)\} - n_c\{H^v_{w,a} - H^l_{w,a}\}(x)\frac{dM^l_{w,a}(x)}{dx} - n_c\{H^v_{w,c} - H^l_{w,c}\}(x)\frac{dM^l_{w,c}(x)}{dx} + n_c h\left\{\left\{\frac{\Delta S_{H_2}}{2F} + \frac{\Delta S_{O_2}}{4F}\right\}\{T_s(x) + 273\} - \eta(x)\right\}I(x) \quad [T\text{-}10]$$

Bulk temperature

$$T_b = T^0_b \quad \text{for constant temperature} \quad [T\text{-}11a]$$

$$MC_p\frac{dT_{hef}(x)}{dx} = U_b A_b\{T_s(x) - T_{hef}(x)\} \quad \text{for coflow heat exchanger} \quad [T\text{-}11b]$$

$$MC_p\frac{dT_{hef}(x)}{dx} = -U_b A_b\{T_s(x) - T_{hef}(x)\} \quad \text{for counterflow heat exchanger} \quad [T\text{-}11c]$$

Local current density

$$I(x) = \frac{\sigma_m(x)}{t_m}\{V_{oc} - V_{cell} - \eta(x) \quad [T\text{-}12]$$

$$\text{At } x = L \quad \frac{dT_s(x)}{dx} = \frac{U_b}{k}\{T_b - T_s(x)\} \qquad [10]$$

At the inlet point (Eq. 9), when the initial temperatures of the solid layer and the injected liquid water are different, it is assumed that energy is immediately exchanged between them to allow both to reach the same temperature. The second and third terms on the right side of Eq. 9 represent the energy transport between the liquid in the channels and the solid layer. The first terms on the right side of Eq. 9 and 10 represent the heat transport between the solid layer and surrounding the solid area normal to the inlet and outlet flow direction.

Solution techniques.—These equations are solved simultaneously using a finite difference algorithm called BAND (J) proposed by Ref. 16. For a specified average current density I_{avg}, a guessed value for the cell potential is chosen, and the model equations are solved to get a set of local current densities $I(x)$ and I_{avg} using the following equation

$$I_{avg} = \frac{1}{L}\int_0^L I(x)dx \qquad [11]$$

where L is the channel length. If the calculated I_{avg} is not equal to the specified I_{avg}, a different cell potential is chosen. This process is repeated until the calculated I_{avg} agrees with the specified I_{avg} to within a tolerable range. Instead of iterating the model manually, an iteration loop based on the Newton-Raphson method is used to help search for the correct cell potential. The procedure for this Newton-Raphson based search method is given in Ref. 6.

Results and Discussion

Proper water and thermal management has been found to be essential to achieving high performance at high efficiency for PEM fuel cells. Consequently, in the search for designs and operating strategies and conditions that will yield optimal fuel cell performance, an accurate computer model of the system is very useful and cost effective. In this section, this model will be used to evaluate the effectiveness of some humidification and heat removal strategies and to investigate the effects of various operating conditions on the performance of a PEM fuel cell.

A base case which corresponds to a PEM fuel cell operating with pure hydrogen and oxygen entering at 1 atm abs and 80°C, a surrounding temperature held constant at 70°C, and a current density of 1.1 A/cm^2 is evaluated. The anode inlet stream is saturated with water vapor, and dried oxygen is supplied to cathode. The physical and transport values used represent those of a Nafion of 1100 equivalent weight. The other parameters for the base cases are given in Table II.

Base case.—The results for the base case are shown in Fig. 2-5. Figure 2 shows that as the fluid flows down the channel, the amount of vapor water ($P_{w,a}$) in the anode decreases as the result of the net transport of water from the anode to the cathode. Even though some water is transported by diffusion from the cathode back to the anode, the replenishing rate is not fast enough to maintain a high water content at the anode side of the membrane (see Fig. 3). Consequently, the current densities generated along the channel decrease as the membrane becomes drier and more resistive (see Fig. 5). This membrane drying effect along with the decrease in the water concentration translate to lower depletion rates of hydrogen and oxygen farther down the channels.

Figure 3 illustrates the interesting interaction between two water transport mechanisms in the membrane of a fuel cell: diffusion and electro-osmosis. (Convective transport by a pressure gradient is not present in this case because the anode and cathode pressures are the same.) In the figure, positive values of the number of water molecules per proton denote positive flow from the anode side to the cathode side of membrane. Near the entrance of the fuel cell, the amount of reactants and the partial pressure of water in the anode are high. Consequently, the membrane conductivity is high, and the local current density is also high. Note that the diffusion effect is positive in this region. That is, water is transported from the anode side to the cathode side of the membrane by the diffusion because the anode channel is saturated with water vapor, in contrast to the dried cathode stream. Therefore, having a little bit of the water vapor at the inlet of the cathode stream can improve the cell performance by reducing the amount of water diffused from the

Table II. Values for parameters used in the base case.

Average current density	1.1 A/cm^2
Bulk temperature	70°C
Channel width	0.1 cm
Channel height	0.1 cm
Channel length	10 cm
Number of channel	50
Open-circuit potential	1.1 V
Oxygen exchange current density	0.01 A/cm^2
Condensation rate constant	100 /s
Membrane	
Dry density	2.0 g/cm^3
Dry equivalent weight	1100 g/mol
Thickness	0.01275 cm
Intradiffusion coefficient of water in membrane[a]	5.5×10^{-7} cm^2/s
Water permeability[b]	1.58×10^{-14} cm^2
Water viscosity[c]	3.565×10^{-3} g/cm-s
Anode	
Inlet temperature	80°C
Hydrogen flow rate	$2.0 \times I_{avg}$
Inlet water vapor	Saturated
Inlet water liquid	0
Pressure	1 atm
Cathode	
Inlet temperature	80°C
Oxygen flow rate	$2.0 \times I_{avg}$
Nitrogen flow rate	0
Inlet water vapor	Dry
Inlet water liquid	0
Pressure	1 atm
Solid layer	
Heat transfer coefficient to bulk[d]	0.025 J/s cm^2 °C
Heat transfer coefficient to channel[d]	0.025 J/s cm^2 °C
Thermal conductivity[e]	0.005 J/s cm °C
Heat transfer area to bulk	200 cm^2

[a] Ref. 6.
[b] Ref. 14.
[c] Ref. 17.
[d] Ref. 18.
[e] Ref. 19.

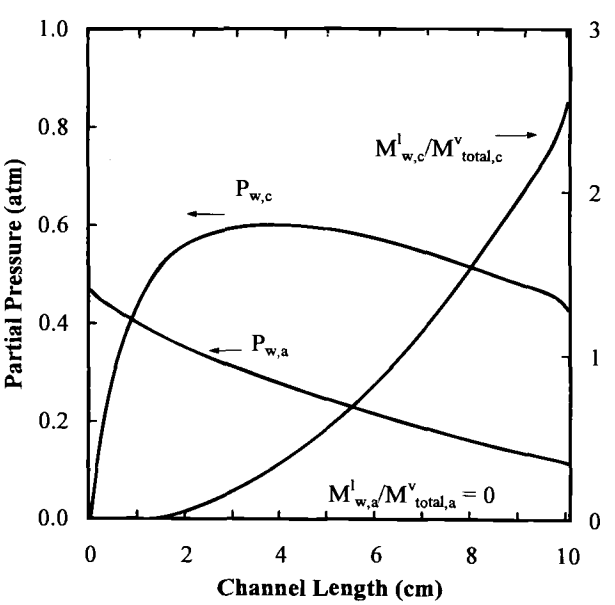

Fig. 2. Water profiles along the flow channels for the base case.

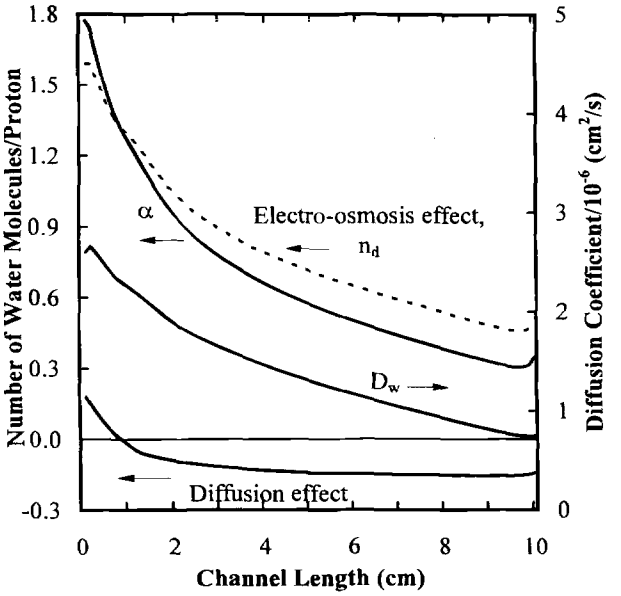

Fig. 3. A comparison of the effects on the net water transport in the membrane and the diffusion coefficient along the channels for the base case.

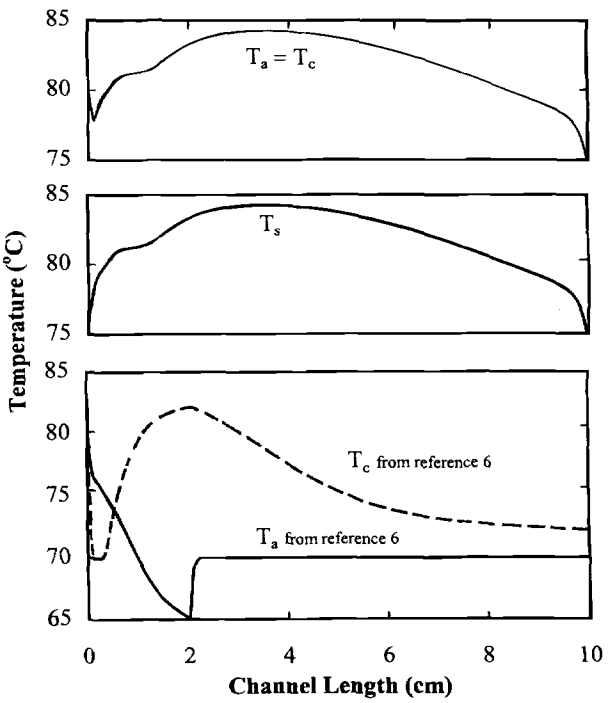

Fig. 4. A comparison of temperature profiles along the channels with the previous model for the base case.

anode side to the cathode side of the membrane. In this region, the water transport rate by electro-osmosis and diffusion results in a net transport of water (see α in Fig. 3) from the anode to the cathode of approximately 1.8 mol of water per mole of protons. Farther down the channels where the membrane becomes drier as the result of lower water concentrations in the anode channel, the membrane conductivity and local current density decrease even though the concentration of hydrogen increases. The diffusion coefficient of water and the electro-osmotic drag coefficient in the membrane also decrease because of their dependences on the water content in the membrane. However, the amount of water diffused from cathode to anode increases because of the higher water concentration gradients now existing between the anode and cathode channels. This combined effect results in a continuous decrease in the net transport rate of water across the membrane to around 0.4 mol of water per mole of proton near the exit, as illustrated by the more gradual drop in the water partial pressure in the anode gas stream. End effects observed in these figures are attributed to the thermal effects of the differences in the temperatures of the fuel cell, gas phase, and surroundings at the entrance and exit of the fuel cells.

Figure 4 shows the temperature distributions along the channels. For the flow rates and heat-transfer conditions chosen in this case, the anode and cathode gas temperatures stay very close to the solid temperature except near the entrance, where they drop rapidly because of the lower bulk temperature. The solid layer temperature starts at a value about halfway between the gas inlet and bulk temperatures at the inlet and heats up quickly because the higher gas temperatures and the energy released by the reactions. Once the solid temperature reaches the gas temperatures, all three temperatures increase as the result of the energy released by the high current density. Beyond about 0.7 cm down the channel, these temperatures begin to level off as the heat generation by the reaction decreases with decreasing current density. However, these temperatures start to increase again at approximately 1.4 cm down the channel where the water vapor in the cathode gas stream having reached saturation begins to condense and release energy to the system (see Fig. 2). Finally, near the outlet, the gas-phase and solid-phase temperatures decrease more rapidly as more energy is transferred to the cooler surroundings.

For comparison purposes, the temperatures and current density distributions along the flow channel obtained from Nguyen and White's model 6 are also included in Fig. 4 and 5. In the previous model, the solid layer of the fuel cell is assumed to be uniform and constant. That is, the heat-transfer rate from the solid phase to the surroundings or a heat exchanger system was assumed to be infinitely high. Therefore, the energy generated by the reaction on the surface of the solid was not considered, and the energy associated with the condensation and evaporation of water was included in the energy balance equation for the gas phase resulting in large changes in gas channel temperatures. These changes in the gas temperatures affect the water content and, consequently, the transport parameters in the membrane. However, they do not affect the electrode kinetics which depend on the solid-phase temperature only. By including the heat-transfer resistance between the gas phase and solid phase, within the solid phase, and between the solid phase and the surroundings, the temperatures in this model are now higher than those from the model in Ref. 6.

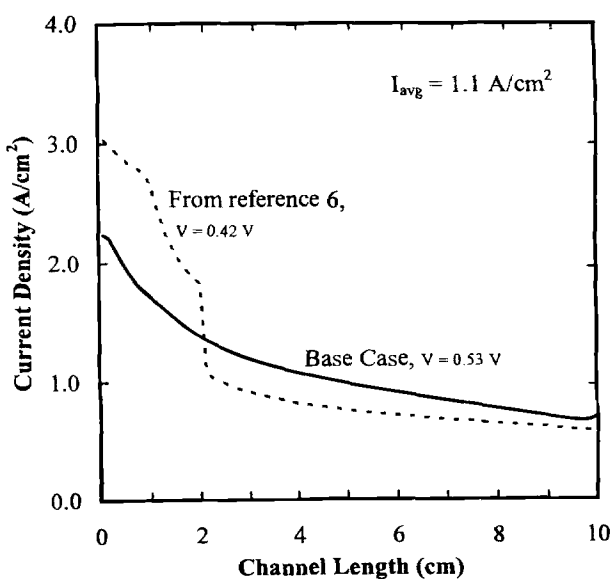

Fig. 5. A comparison of current profiles along the channels with the previous model for the base case.

Since the temperatures no longer go through rapid changes, especially at the region near the inlet, a smoother current density distribution is now observed as compared to the complicated current distribution of Nguyen and White's model (see Fig. 5). Overall, with the solid-phase temperatures and, consequently, the current densities being higher along the whole channel, this model predicts a higher cell potential than that from Ref. 6 for the same operating conditions (0.53 V vs. 0.42 V at I_{avg} = 1.1 A/cm^2). Predictions from the previous model have been regarded to be low relative to experimentally obtained values.

Humidification designs.—As shown in the base case, the anode and consequently its interface with the membrane become less hydrated as the anode gas traverses the channels and loses its water content to the net transport of water across the membrane. One of the approaches often employed by fuel cell designers to overcome the water starvation problem is to raise the humidification temperature. This allows a greater amount of water to be carried into the anode. The model is used here to evaluate the effect of using an anode humidification temperature of 90°C. Other conditions are the same as those of the base case. Figure 6 shows that by increasing the anode humidification temperature from 80 to 90°C the partial pressure of water increases from 0.5 to 0.7 atm, thus allowing more water to be introduced into the fuel cell. As the water vapor enters the cell and encounters the cooler solid temperature of the cell, some condenses (follow $M^l_{w,a}$ in Fig. 6). This condensed liquid water later evaporates as the gas traverses the channel to help keep the membrane hydrated (as shown by a much higher value and more gradual drop of the anode water partial pressure) and more conductive. With the membrane better hydrated and more conductive, this case has not only more uniform current densities along the whole length of the channels (see Fig. 8) but also lower peak current than those of the base case. With the membrane more conductive over a larger length of the channel, the local current densities are higher, eliminating the need for a higher peak current at the entrance and correspondingly a higher cell potential (0.65 V vs. 0.53 V for the base case). Finally, the solid-phase temperature is also more uniform and consistently higher giving rise to a lower kinetic resistance and higher membrane conductivity and water back-diffusion rate. The sharp increase in the solid-phase temperature near the entrance is attributed to the hotter incoming reactant gas and the energy released from the condensation of water as the incoming gas cools.

Another method that can be used to increase the anode humidification level is by liquid water injection. The effectiveness of the liquid injection humidification design is evaluated next using this model. In this case, an additional amount of 80°C liquid water equivalent to 20% the amount of hydrogen in the feed stream is injected into a hydrogen gas stream saturated with water at the same temperature as the base case (80°C). Compared to the base case, the liquid injection case has higher water vapor partial pressure over the whole length of the channels (see Fig. 7). Although not as high as that in the case with the higher humidification temperature, this slightly higher water vapor level still results in an improvement of 0.05 V over the base case (see Fig. 8). The lower solid-phase temperatures in the region near the entrance of the cell are attributed to the loss in energy required to vaporize the liquid water. More water could be injected to maintain higher hydration levels. However, unless the energy needed to vaporize the water is available or the heat-transfer rate between the phases is very high, injecting more liquid water will never give this case, a performance equal to that of the higher humidification temperature case. This is because of the higher energy content associated with carrying water vapor as compared to liquid water.

Figure 9 shows the polarization curves for the three different humidification cases discussed in the previous paragraphs. Note that at low current densities where the performances are kinetically controlled there are no differences between these humidification designs. However, at higher current densities where the effect of the membrane ionic resistance is significantly higher, the advantages of having an optimal water management system becomes obvious, as shown by the higher potentials of the cases with better humidification. The effects of liquid water injection have been experimentally demonstrated in our laboratory.[20] Experimental results from runs at conditions similar to those simulated here are included in Fig. 9 to prove that injecting liquid water into the anode gas stream improves the cell performance, especially at higher current density, thus validating the model predictions. Note that since these data points are not IR-corrected and include overpotential contributed by the anode, which is neglected in this model, the experimental potentials are lower than those predicted by the model. Finally, the sharp drop in potential associated with the mass-transport limitation region is not observed in these polarization curves because the effects of reactant gas transport resistance in the porous electrodes are neglected in this model.

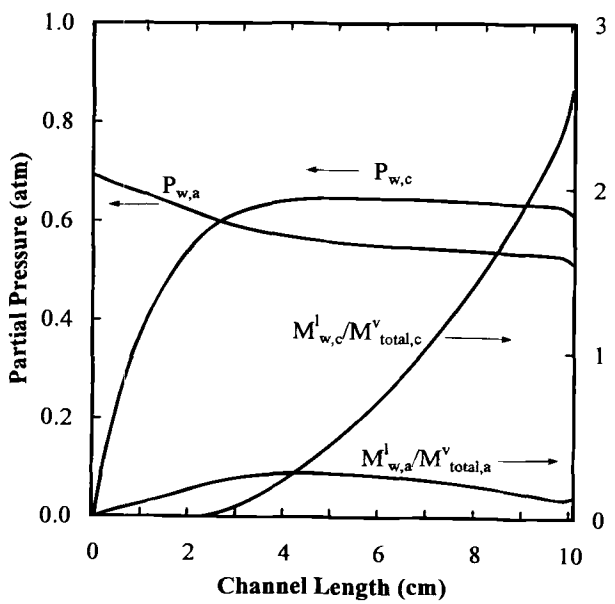

Fig. 6. Water profiles along the channels for the $T_a = T_c$ = 90°C case.

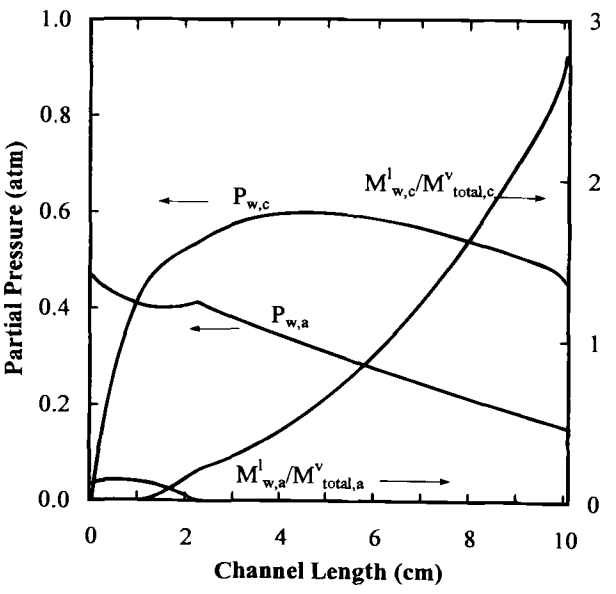

Fig. 7. Water profiles along the channels for the liquid injection case.

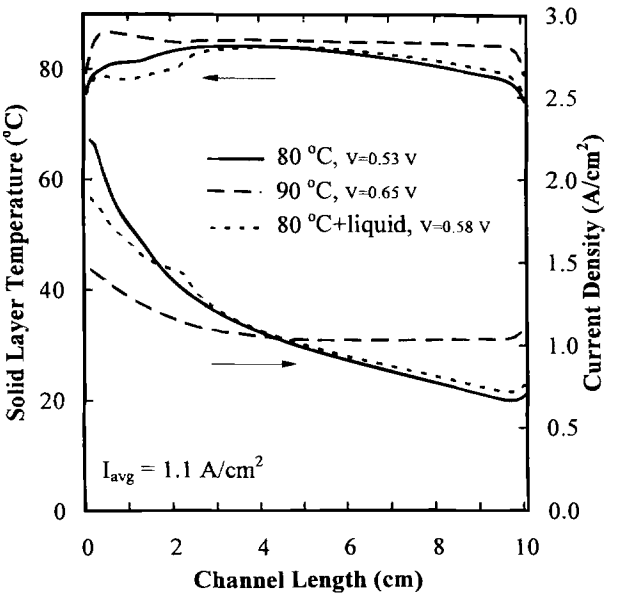

Fig. 8. A comparison of three different humidification designs on the current densities and solid layer temperatures along the channels.

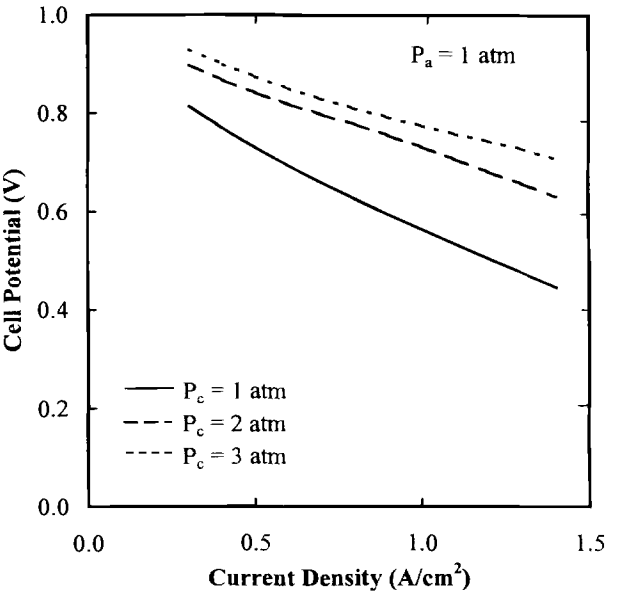

Fig. 10. The effect of convective flow by differential pressure in the membrane on the performance of a PEM fuel cell.

Effect of differential pressure.—As shown in Fig. 3, net water transport in the membrane arises from three mechanisms: electro-osmosis, diffusion, and convention. At low current densities, back-diffusion of water from the cathode to the anode may be sufficient to keep the anode side of the membrane hydrated. At higher current densities where water back-diffusion is insufficient to replenish the water loss from the anode by electro-osmosis, convective water transport from the cathode to the anode by differential pressure could be used. With the anode gas maintained at 1 atm, two different pressure levels, 2 and 3 atm, for the cathode are evaluated using this model. Other conditions are identical to those of the base case. Figure 10 shows the effectiveness of having a higher cathode pressure on the performance of a PEM fuel cell at various current densities. A higher pressure difference yields higher cell performance over the entire range of current densities investigated. Increasing the cathode pressure from 1 to 2 atm yields a larger increase in cell potential than that from 2 to 3 atm. Furthermore, the effects are more significant at higher current densities. This behavior is attributed to the fact that as the membrane becomes better hydrated with more convective flow of water from the cathode to the anode, the membrane resistance due to dehydration becomes less influential than activation resistance. Furthermore, convective flow contributes more at higher current densities where the effect of electro-osmosis is higher. Figure 11 shows the contribution by each water transport mechanism along the channels for the case where the pressure of the anode and cathode gases are at 1 and 2 atm, respectively. Comparing the curves in Fig. 11 to those in Fig. 3 shows that the contribution from water back diffusion is about the same. However, the water transport rate by electro-osmosis can be maintained at a high level because the convection flow of water from the cathode to the anode helps to keep the membrane well

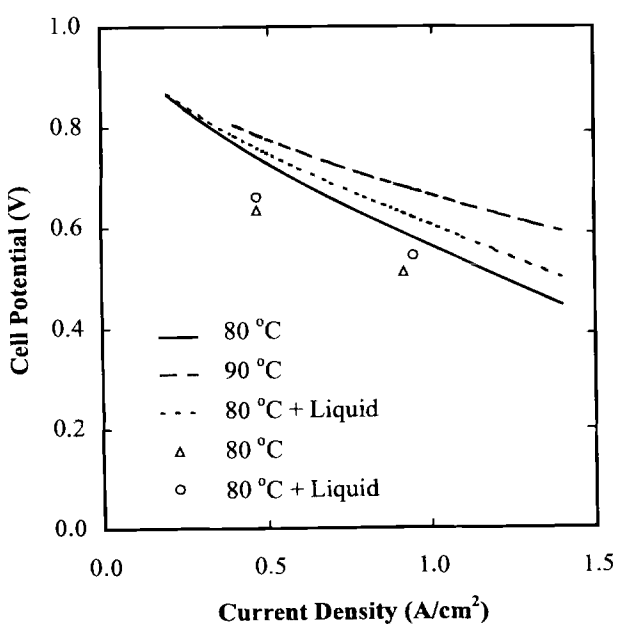

Fig. 9. The effect of humidification designs on the performance of a PEM fuel cell. Lines are the model results, and dots are non-IR corrected experimental results from Ref. 20.

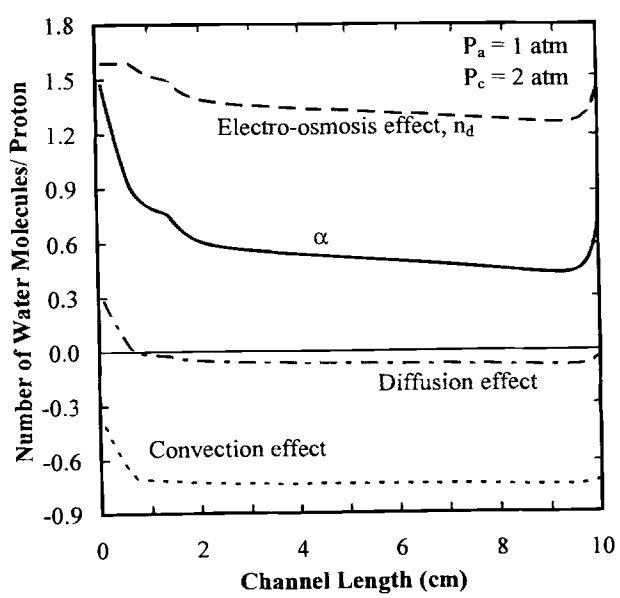

Fig. 11. A comparison of the effects on water transport in the membrane along the channels for the P_a = 1 atm and P_c = 2 atm case.

hydrated and more conductive. Initially, little water exits in the cathode to take advantage of the pressure gradient. Therefore, the convection effect starts at a low 0.4 molecule of water per proton level in this front region. As more water is available along the channels, the convective effect increases rapidly and stays constant at about 0.9 molecule of water per proton. At this level, the decrease in the net water transport is governed by the decrease in the electro-osmosis effect as a result of lower water concentrations in the anode channels. Near the end of the channels, the electro-osmosis effect increases because of the temperature decrease caused by the energy loss to the bulk at the end of the channels. This end effect also contributes to the increase in the net water transport coefficient in the region. In summary, a higher cathode gas pressure can be used to reduce the anode dehydration problem and improve the fuel cell performance. However, the energy and equipment cost of compressing the cathode gas, especially air, and the effect of oxygen gas crossing over to the anode must also be considered.

Effect of temperatures.—Figure 12 shows the effect of the bulk temperature on the cell potential of PEM fuel cells when I_{avg} is held at 1.1 A/cm^2. The anode and cathode gas stream temperatures are equally maintained, and the results from three different temperatures are plotted. When the bulk temperature increases, the potential shows convexity. Increases in the cell potential at lower temperatures are caused by increases of the transport properties, D_w, n_d, and σ_m, of the membrane and the decreases of kinetic resistance. After the cell potential reaches a maximum value, overheating causes the overpotential to increase and the potential to decrease. It is desirable to have heat removal schemes when the bulk temperature extends beyond the optimum values. Within the investigated temperature range, it is found that the cell potential increases with the gas inlet temperature. This happens primarily because more humidified gases are injected with an increases of gas inlet temperatures as mentioned previously, even though the overpotential increases. As the gas stream inlet temperatures increase, the optimum bulk temperature decreases to remove the excess energy that is supplied from the inlet gas streams.

Heat exchanger designs.—A heat exchanger can be used not only to remove energy from the cell but also to distribute it more effectively along the channel. Two types of exchangers are considered: coflow and counterflow respective to the gas stream, to study the effect of energy distribution. The temperature profiles of the solid-layer and heat exchanger fluid along the channel for both types of heat exchanger schemes in contrast to the case in which convective heat transfer is used with a constant bulk temperature are shown in Fig. 13. Liquid water is used for the heat exchanger fluid. The heat exchanger fluid inlet temperature is chosen so that the average heat exchanger fluid temperature is equal to the constant bulk temperature for the convective heat removal case. As shown in the figure, the coflow heat exchanger takes energy from the front section of the channels and releases it to the end section, while the counterflow does so inversely. Consequently, the solid layer shows higher temperatures at the front section with the counterflow heat exchanger and at the end section with the coflow heat exchanger as compared to that with the constant bulk temperature condition. Even though the temperature of the solid layer is higher at the end region using the coflow exchanger, the energy is not used properly because water content limits the performance of the cell in that region. Meanwhile, in the counterflow case, the unused energy at the end region is taken to the front to maintain higher partial pressures of water in the anode gas stream (see Fig. 14). As a result, the cell performance with the counterflow setup is better while that with the coflow is worse than the case without a heat exchanger (see Fig. 15).

To study the effect of heat removal, the cell potential vs. the averaged heat exchanger fluid temperature for two different heat exchanger flow rates is shown in Fig. 15 for a gas stream temperature of 80°C and an average current density of 1.1 A/cm^2. In the figure, a lower flow rate of heat exchanger fluid corresponds to a higher heat removal effectiveness. As the flow rate of the heat exchanger fluid decreases, more energy is transferred along the cell, making the energy distribution effect on the cell performance more significant. Therefore, higher heat transfer improves the cell performance for the counterflow heat exchanger case but worsens it for the coflow heat exchanger. Also, for the counterflow heat exchanger the maximum average bulk temperature decreases with decreases in the heat exchanger fluid flow rate because the energy is used more effectively. On the other hand, for the coflow heat exchanger the maximum average bulk temperature increases with decreases in the heat exchanger fluid flow rate due to the insufficient use of energy at the end region of the flow channel.

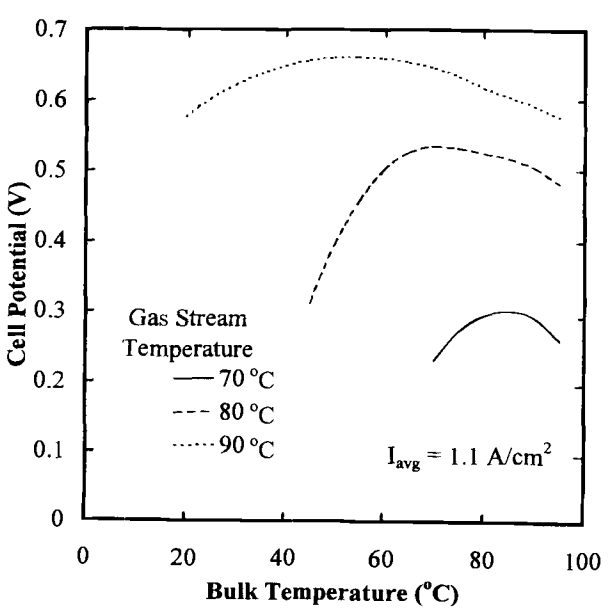

Fig. 12. The effect of bulk temperatures on the performance of a PEM fuel cell for different gas stream temperatures when I_{avg} = 1.1 A/cm^2.

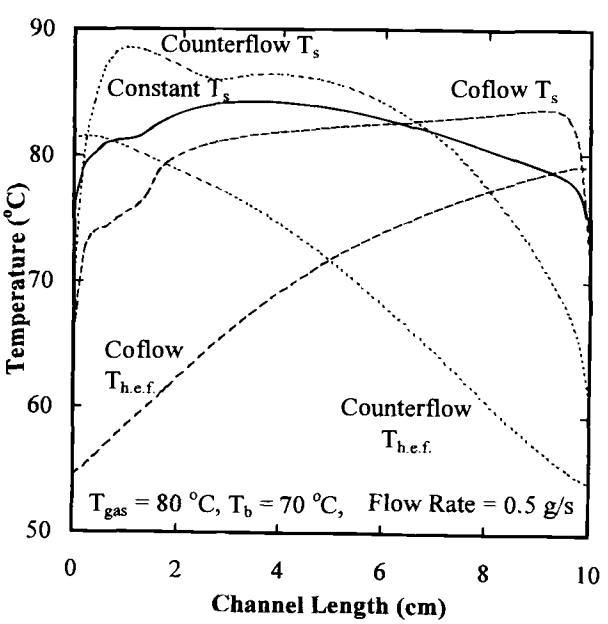

Fig. 13. Temperature profiles of solid layer and heat exchanger fluid for different bulk designs when T_{gas} = 80°C, T_b = 70°C, flow rate of heat exchanger fluid = 0.5 g water/s, and I_{avg} = 1.1 A/cm^2.

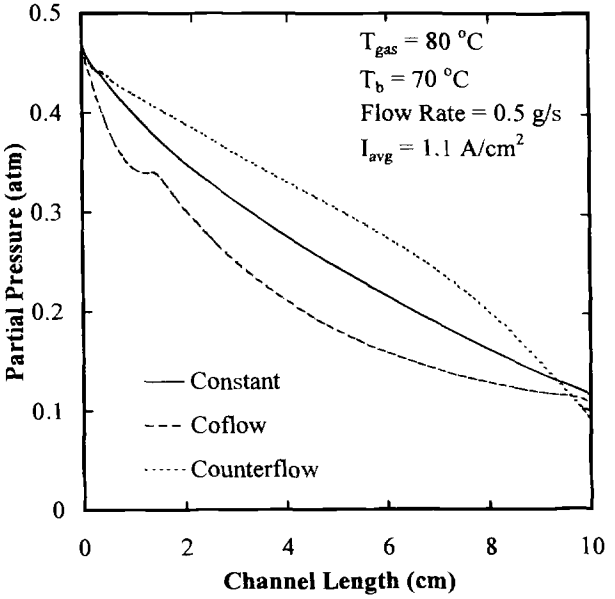

Fig. 14. Vapor water profiles along the flow channels for different bulk designs when T_{gas} = 80°C, T_b = 70°C, flow rate of heat exchanger fluid = 0.5 g water/s, and I_{avg} = 1.1 A/cm^2.

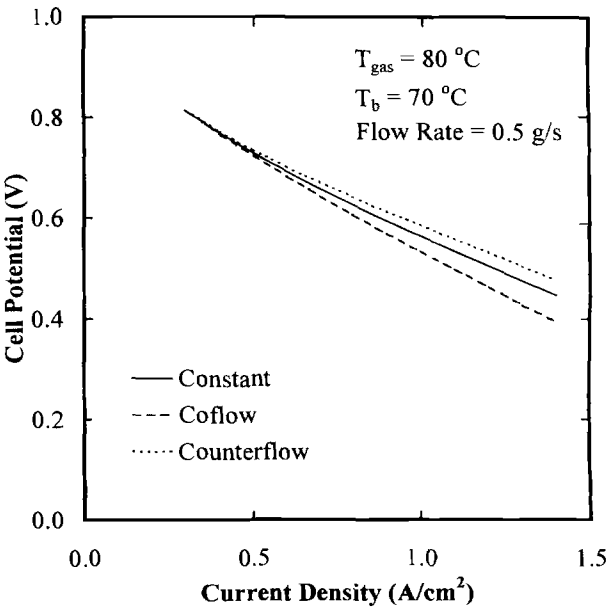

Fig. 16. The effect of bulk designs on the performance of a PEM fuel cell.

Figure 16 shows the polarization curves for the two different heat exchanger designs as compared to the constant bulk temperature case. The results illustrate that better performance will be obtained with the counterflow heat exchanger for most regions of current density investigated. Note that, at low current densities where the performance is kinetically controlled, there are no differences among the heat removal designs. However, at higher current densities, the advantages of having better heat removal and distribution design become obvious, as shown by the higher potentials of the cases with the counterflow heat exchanger. Figure 17 shows that the improvement in the current density at fixed cell potential obtained with the counterflow heat exchanger is achieved mainly at the end regions of the channels, and it also shows the most uniform distribution of current densities along the channel.

Conclusions

An along-the-channel model for a proton exchange membrane fuel cell was developed in which the energy balance of the solid phase and convective water transport by differential pressure were included. The model was used to evaluate the effectiveness of various humidification designs, higher cathode gas pressure, and heat removal schemes for PEM fuel cells. The results show that humidification of the anode gas is required to improve the conductivity of the membrane, and the liquid after injection and higher humidification temperature can improve the cell performance by introducing more water into the anode. Also, applying higher cathode gas pressure helps to replenish the water loss by electroosmosis, thereby making the membrane more conductive and thus resulting in higher cell performance. Finally, the counterflow heat exchanger is more effective than both the coflow scheme and the constant bulk temperature.

The model presented here can be used to evaluate the effectiveness of different operating strategies and designs,

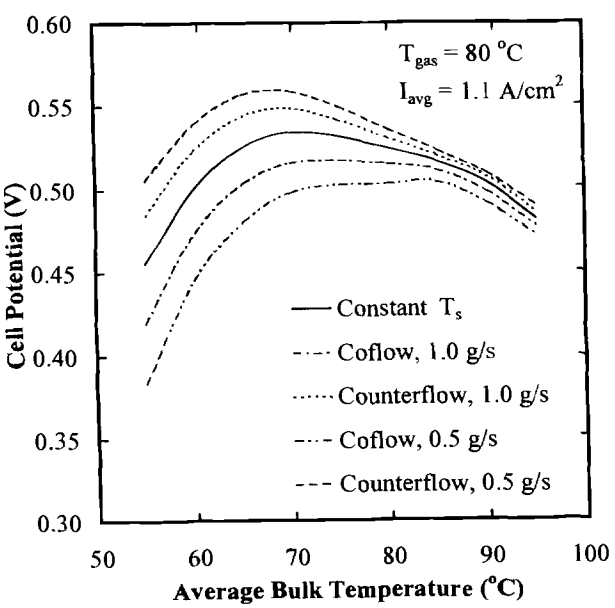

Fig. 15. Effect of heat exchanger design for the average bulk temperature with two different heat exchanger fluid flow rates when T_{gas} = 80°C and I_{avg} = 1.1 A/cm^2.

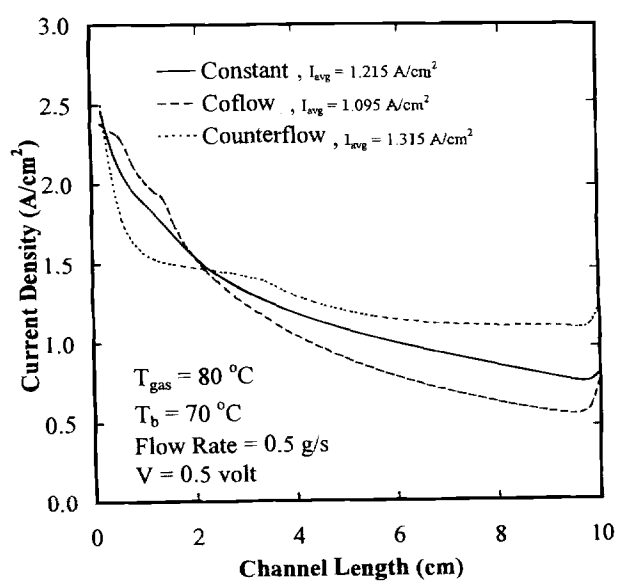

Fig. 17. A comparison of three different bulk designs on the current densities along the channels.

and these results can then be used to help determine an optimal fuel cell design for a specific application.

Acknowledgments

The authors wish to acknowledge the financial support of this work by the Delphi Automotive Systems of General Motors Corp. (PO No. RPS35101), the Department of Energy (Contract DE-AC02-90CH10435), and the KSTAR NSF-EPSCoR Program.

Manuscript submitted August 28, 1997; revised manuscript received November 21, 1997.

The University of Kansas assisted in meeting the publication costs of this article.

LIST OF SYMBOLS

a heat-transfer length between channel to solid layer per unit area, cm
a_k activity of water in stream k
A_b heat transfer length between solid layer to bulk per unit area, cm
A_s conductive heat-transfer area of solid layer per unit area, cm^2
c_w concentration of water in the membrane, mol/cm^3
$c_{w,k}$ concentration of water at k interface of the membrane, mol/cm^3
C_p heat capacity of heat exchanger fluid, J/mol °C
$C_{p,i}$ heat capacity of species i, J/mol °C
d channel height, cm
D^0 intradiffusion coefficient of water in membrane, cm^2/s
D_w effective diffusion coefficient of water in the membrane, cm^2/s
F Faraday constant, 96,487 C/equiv
h channel width, cm
$H_{w,k}$ enthalpy of water vapor or liquid in k stream, J/mol
I local current density, A/cm^2
I^0 exchange current density for the oxygen reaction, A/cm^2
I_{avg} average current density, A/cm^2
k thermal conductivity of solid layer, J/s cm °C
k_c condensation rate constant, s^{-1}
k_p hydraulic permeability of water in membrane, cm^2
L cell channel length, cm
M molar flow rate of heat exchanger fluid, mol/s
M_i molar flow rate of species i, mol/s
$M_{m,dry}$ equivalent weight of a dry membrane, g/mol
n_c number of channel for each side of membrane
n_d electro-osmotic drag coefficient
$N_{i,y,k}$ Y component molar flux of species in k channel, $mol/s\text{-}cm^2$
$N^v_{w,y,k}$ Y component molar flux of water vapor in k channel, $mol/s\text{-}cm^2$
P_i partial pressure of species i, atm
P_k total pressure of channel k, atm
P_w partial pressure of water in the membrane, atm
$P_{w,k}$ vapor pressure of water in k channel, atm
R gas constant, 82.06 cm^3 atm/mol K or 8.314 J/mol K
SH cell height, cm
SW cell width, cm
t_m membrane thickness, cm
T_b bulk temperature or heat exchanger fluid temperature, °C
T_k temperature of k stream, °C
U overall heat-transfer coefficient between channel and solid layer, $J/s\ cm^2$ °C
U_b overall heat-transfer coefficient between solid layer and bulk or between solid body and heat exchanger fluid, $J/s\ cm^2$ °C
V_{oc} cell open-circuit potential, V
V_{cell} cell potential, V
x direction along the channel length, cm
y direction normal to the channel length, cm

Greek

α net water transfer coefficient per proton
δ step size for the potential
ΔS_i change of entropy for the i species reaction on platinum, J/mol K
η overpotential for the oxygen reaction, V
μ water viscosity, g/cm s
λ water contents of membrane
$\rho_{m,dry}$ density of a dry membrane, g/cm^3
σ_m membrane conductivity, S/cm

Subscripts and superscripts

a anode
c cathode
calc calculated
guess guessed
H_2 hydrogen
inert inert gas
k anode or cathode channel
l liquid
n iteration number
sat saturation
spec specified
v vapor
w water
o initial condition

REFERENCES

1. E. A. Ticianelli, C. R. Derouin, A. Redondo, and S. Srinivasan, *J. Electrochem. Soc.*, **135**, 2209 (1988).
2. J. M. J. Blomen and M. N. Mugerwa, *Fuel Cell Systems*, Plenum Press, New York (1993).
3. D. P. Wilkinson, H. H. Voss, and K. Prater, *J. Power Sources*, **49**, 117 (1994).
4. N. E. Vanderborgh, J. Hedstrom, and J. R. Huff, in *Proceedings of 25th IECEC*, p 3.149, Reno, NV (1990).
5. R. Mosdale and S. Srinivasan, *Electrochim. Acta*, **40**, 413 (1995).
6. T. V. Nguyen and Ralph E. White, *J. Electrochem. Soc.*, **140**, 2178 (1993).
7. M. Watanabe, Y. Satoh, and C. Shimura, *J. Electrochem. Soc.*, **140**, 3190 (1993).
8. D. M. Bernardi and M. W. Verbrugge, *J. Electrochem. Soc.*, **139**, 2477 (1992).
9. J. C. Amphlett, R. M. Baumert, R. F. Mann, B. A. Peppley, P. R. Roberge, and T. J. Harris, *J. Electrochem. Soc.*, **142**, 1 (1995).
10. J. C. Amphlett, R. M. Baumert, R. F. Mann, B. A. Peppley, P. R. Roberge, and T. J. Harris, *J. Electrochem. Soc.*, **142**, 9 (1995).
11. T. E. Springer, T. A. Zawodzinski, and S. Gottesfeld, *J. Electrochem. Soc.*, **138**, 2334 (1991).
12. T. F. Fuller and J. Newman, *J. Electrochem. Soc.*, **140**, 1218 (1993).
13. M. Kimble and N. E. Vanderborgh, in *Proceedings of the 27th IECEC*, p. 3.413, San Diego, CA (1992).
14. J. L. Fales, N. E. Vanderborgh, and P. Stroeve, in *Diaphragms, Separators, and Ion-Exchange Membranes*, J. W. van Zee, R. W. White, K. Kinoshita, and H. S. Burney, Editors, PV 86-13, p 179, The Electrochemical Society Proceedings Series, Pennington, NJ (1986).
15. T. A. Zawodzinski, T. E. Springer, J. Davey, J. Valerio, and S. Gottesfeld, in *Modeling of Batteries and Fuel Cells*, R. E. White, M. Verbrugge, and J. S. Stuckel, Editors, PV 91-10, p 187, The Electrochemical Society Proceeding Series, Pennington, NJ (1991).
16. J. S. Newman, *Electrochemical Systems*, Prentice-Hill, Inc., Englewood Cliffs, NJ (1991).
17. *Handbook of Chemistry and Physics*, 70th ed., R. C. Weast, Editor, Boca Raton, FL (1989).
18. N. E. Vanderborgh, Private communication, 1995.
19. J. P. Holman, *Heat, Transfer*, McGraw-Hill, Inc., New York (1986).
20. D. L. Wood and T. V. Nguyen, Abstract 187, p 224, The Electrochemical Society Meeting Abstracts, Vol. 97-2, Paris, France, Aug 31-Sept 5, 1997.